

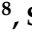



Article

Green Synthesis and Photocatalytic Dye Degradation Activity of CuO Nanoparticles

Sadia Aroob ¹, Sónia A. C. Carabineiro ^{2,*} , Muhammad Babar Taj ^{1,*} , Ismat Bibi ¹, Ahmad Raheel ³, Tariq Javed ⁴, Rana Yahya ⁵, Walla Alelwani ⁶, Francis Verpoort ⁷ , Khanita Kamwilaisak ⁸, Saleh Al-Farraj ⁹ and Mika Sillanpää ^{10,11,*} 

¹ Institute of Chemistry, The Islamia University of Bahawalpur, Bahawalpur 63100, Pakistan

² LAQV-REQUIMTE, Department of Chemistry, NOVA School of Science and Technology, Universidade NOVA de Lisboa, 2829-516 Caparica, Portugal

³ Department of Chemistry, Quaid-e-Azam University, Islamabad 44000, Pakistan

⁴ Department of Chemistry, University of Sahiwal, Sahiwal 57000, Pakistan

⁵ Department of Chemistry, College of Science, University of Jeddah, Jeddah 23218, Saudi Arabia

⁶ Department of Biochemistry, College of Science, University of Jeddah, Jeddah 23218, Saudi Arabia

⁷ State Key Laboratory of Advanced Technology for Materials Synthesis and Processing, Wuhan University of Technology, Wuhan 430070, China

⁸ Department of Chemical Engineering, Faculty of Engineering, Khon Kaen University, Khon Kaen 40002, Thailand

⁹ Department of Zoology, College of Science, King Saud University, Riyadh 11362, Saudi Arabia

¹⁰ Department of Biological and Chemical Engineering, Aarhus University, Nørrebrogade 44, 8000 Aarhus C, Denmark

¹¹ Department of Chemical Engineering, School of Mining, Metallurgy and Chemical Engineering, University of Johannesburg, P.O. Box 17011, Doornfontein 2028, South Africa

* Correspondence: sonia.carabineiro@fct.unl.pt (S.A.C.C.); dr.taj@iub.edu.pk (M.B.T.); mikasillanpaa@gmail.com (M.S.)



Citation: Aroob, S.; Carabineiro, S.A.C.; Taj, M.B.; Bibi, I.; Raheel, A.; Javed, T.; Yahya, R.; Alelwani, W.; Verpoort, F.; Kamwilaisak, K.; et al. Green Synthesis and Photocatalytic Dye Degradation Activity of CuO Nanoparticles. *Catalysts* **2023**, *13*, 502. <https://doi.org/10.3390/catal13030502>

Academic Editor: Weilin Dai

Received: 20 January 2023

Revised: 17 February 2023

Accepted: 20 February 2023

Published: 28 February 2023



Copyright: © 2023 by the authors. Licensee MDPI, Basel, Switzerland. This article is an open access article distributed under the terms and conditions of the Creative Commons Attribution (CC BY) license (<https://creativecommons.org/licenses/by/4.0/>).

Abstract: The degradation of dyes is a difficult task due to their persistent and stable nature; therefore, developing materials with desirable properties to degrade dyes is an important area of research. In the present study, we propose a simple, one-pot mechanochemical approach to synthesize CuO nanoparticles (NPs) using the leaf extract of *Seriphidium oliverianum*, as a reducing and stabilizing agent. The CuO NPs were characterized via X-ray diffraction (XRD), scanning electron microscopy (SEM), photoluminescence (PL) and Fourier-transform infrared spectroscopy (FTIR). The photocatalytic activity of CuO NPs was monitored using ultraviolet-visible (UV-Vis) spectroscopy. The CuO NPs exhibited high potential for the degradation of water-soluble industrial dyes. The degradation rates for methyl green (MG) and methyl orange (MO) were $65.231\% \pm 0.242$ and $65.078\% \pm 0.392$, respectively. Bio-mechanochemically synthesized CuO NPs proved to be good candidates for efficiently removing dyes from water.

Keywords: photocatalysis; degradation; copper oxide; nanoparticles; methyl green; methyl orange; dyes; wastewater; biomimetic; environmentally benign; photochemical; purification; waste management

1. Introduction

The development of industrialization has increased the risk of environmental pollution [1,2]. Several types of waste can seriously threaten water bodies [3,4]. Organic dyes are significant pollutants produced by different industries, such as food, pharmaceutical, leather, textile, inks, cosmetics, etc. [5–7]. Every year, tons of complex dyes are formed and discharged into water bodies, which cause harmful effects on aquatic life [8–10]. Developing methods for degrading dyes is a challenge for researchers [11–15]. Some of these methods are ion exchange, chemical oxidation, ozonolysis, photocatalytic degradation, and coagulation-based techniques [16–21]. Adsorption is often used to remove several

water pollutants [22–34]. However, photocatalytic degradation using a semiconductor photocatalyst is considered a cost-effective and green approach to successfully degrade dyes [35–39].

Light active materials with large surface areas are needed to degrade organic dyes [40,41]. Several metal oxides or semiconductors are active photocatalysts under sunlight, due to their small band gap [42,43]. CuO is a p-type semiconductor having a narrow band gap of 2.1 to 2.71 eV [44]. CuO nanoparticles (NPs) show a proper response towards optical, mechanical, and photolytic applications [42,45–47]. Different methods are used to synthesize CuO NPs, including sol-gel, solvothermal, microwave irradiation, hydrothermal, arc discharge, etc. [48,49].

The synthesis of CuO NPs using plant extracts is considered the most practical and green approach [50,51]. Different biological methods for synthesizing CuO NPs involve the use of bacteria, fungi, algae, and plants as bioactive materials by using leaves, flowers, or stem extracts, including *Solanum americanum*, *Solanum nigrum*, *Camellia japonica*, *Pterispermum acerifolium*, *Gum karaya*, Soya bean, etc. [38,51–53].

Several efforts were made to understand the biological mechanism and phytochemicals involved in the green synthesis of CuO NPs and their characteristics [54]. Different biomolecules responsible for stabilizing and reducing nanoparticles can be amino acids, proteins/enzymes, alkaloids, polysaccharides, vitamins, and alcoholic compounds [55,56]. The prepared CuO NPs depend on the reduction power of ions and the reduction capability of plants having biochemicals such as polyphenols, enzymes, and other chelating agents [57,58].

Seriphidium oliverianum belongs to the family Asteraceae, widely used in folk medicines [59,60]. It has many active biomolecules, such as cardenolides, anthraquinones, tannins, alkaloids, flavonoids, terpenoids, phenolic acids, and carbohydrates [61]. The biological CuO NPs can be effectively reduced by biomolecules [62].

Catalysis-based processes play a crucial role in producing high-value goods such as fuel, chemicals, pharmaceuticals, etc., from cheap raw materials. Catalysts are considered the engines behind these processes [63]. It is projected that the catalysis-based sector may produce commodities worth several trillion euros annually, with a total sales value of catalytic materials of about 20 billion euros, highlighting the importance of catalysis to our community [64]. The chemical industry mainly uses heterogeneous catalysis for several reasons, such as simple catalyst separation, durability, and suitability for continuous operation. However, the designing of catalyst materials is not a straightforward process due to their complex architecture and the poor understanding of active centers [65]. This idea becomes exceptionally crucial for the consistent mass production of solid catalysts. Despite the advanced level of technology in this sector, catalyst synthesis is often seen as more of an art than a science. Therefore, a significant amount of research focuses on the creation of catalysts, which is an indication of the tremendous effort put into understanding the rational synthesis of active, selective, and stable catalysts. This idea is crucial for the consistent mass production of solid catalysts. Consequently, despite the advanced level of technology in this sector, catalyst synthesis is frequently seen as more of an art than a science. Therefore, it is not surprising that there is much research focusing on the creation of catalysts, as they attest to the tremendous effort put into understanding the logical synthesis of active, selective, and stable catalysts [66,67].

Precipitation, deposition–precipitation, the hydrothermal approach, and impregnation are the main pathways for synthesizing industrial-scale catalysts that are currently developed to ensure a reasonable level of control over the catalyst properties and performance [68]. Other methods such as solid-state reactions and fusing can also be used. However, solution-based procedures always generate a significant amount of solvent waste due to their inherent nature. In addition, nitrate or chloride metal salts are commonly used as precursors, which may result in the production of poisonous gases during subsequent calcination stages. Necessary measures may be required to prevent these gases from escaping into the atmosphere [69]. Wet chemistry procedures are also frequently viewed as

tedious and challenging to scale up for a particular formulation of the catalytic material. Furthermore, due to their energy requirements and possible role as producers of hazardous waste, solution processes and additional treatment stages, carried out at high temperatures, frequently fail to fulfill current environmental standards. Thus, there is a large interest in creating alternative synthetic procedures that are less harmful to the environment, easier, more economical, more productive, and scalable.

Superior features of the generated materials and more advantageous economic or environmental factors of the processes can stimulate the creation of innovative synthetic techniques. Due to the growing urgency of environmental issues and energy depletion resources, environmentally friendly production techniques of catalyst synthesis are particularly advantageous [70]. Reactive extrusion and ball milling are two prominent, quick, and efficient mechanochemical processes to create catalytic materials.

In the last decades, the mechanochemical approach was developed as a sustainable method for the large-scale production of various nanomaterials [71]. This procedure can generate well-dispersed metal oxide nanoparticles to be used in wide-ranging applications, including environmental monitoring, energy storage, conversion, or biomedical uses. The mechanochemical synthesis is relatively simple, easy to scale-up and create a uniform reaction [71]. The motivation of work is that chemical reactions can proceed in the absence of excess solvents or heating, making this a key reason for the recent interest in green chemistry.

To the best of our knowledge, the mechanical synthesis of CuO NPs using *Seriphidium oliverianum* extract was not yet reported in the literature. In this study, we develop a straightforward bio-mechanochemical approach using an electric mortar grinder mill to synthesize CuO NPs in the presence of *Seriphidium oliverianum* leaf extract. We also evaluated the degradation efficiency of water-soluble dyes, namely methyl green (MG) and methyl orange (MO).

2. Results and Discussion

2.1. X-ray Diffraction (XRD)

XRD was employed to study and explore the crystalline nature of the CuO nanostructured material. The average grain size of the material was obtained using the Debye–Scherrer’s formula:

$$D = k\lambda/\beta \cos \theta \quad (1)$$

where “D” is the crystallite size (nm), “k” is Scherrer’s constant, equal to 0.98, “β” is full width at half maximum (FWHM), and “θ” is the angle of diffraction.

The calculated average crystallite size of the NPs is 12.44 nm. The PXRD diffractogram (Figure 1) displays several characteristics peaks of the monoclinic structure for CuO NPs (standard JCPDS data card no. 00-001-1117 [27]).

2.2. Scanning Electron Microscopy (SEM)

The accumulation of fine CuO nanoparticles originated aggregates. High surface area to volume ratio of nanoparticles provides very high surface energy. To minimize its surface energy, the nanoparticles tend to agglomerate. Uncontrolled agglomeration may occur due to attractive van der Waals forces between particles. The average grain size obtained for CuO NPs was 1.48 μm. Figure 2 shows that the green synthesis of CuO NPs produces small, aggregated particles.

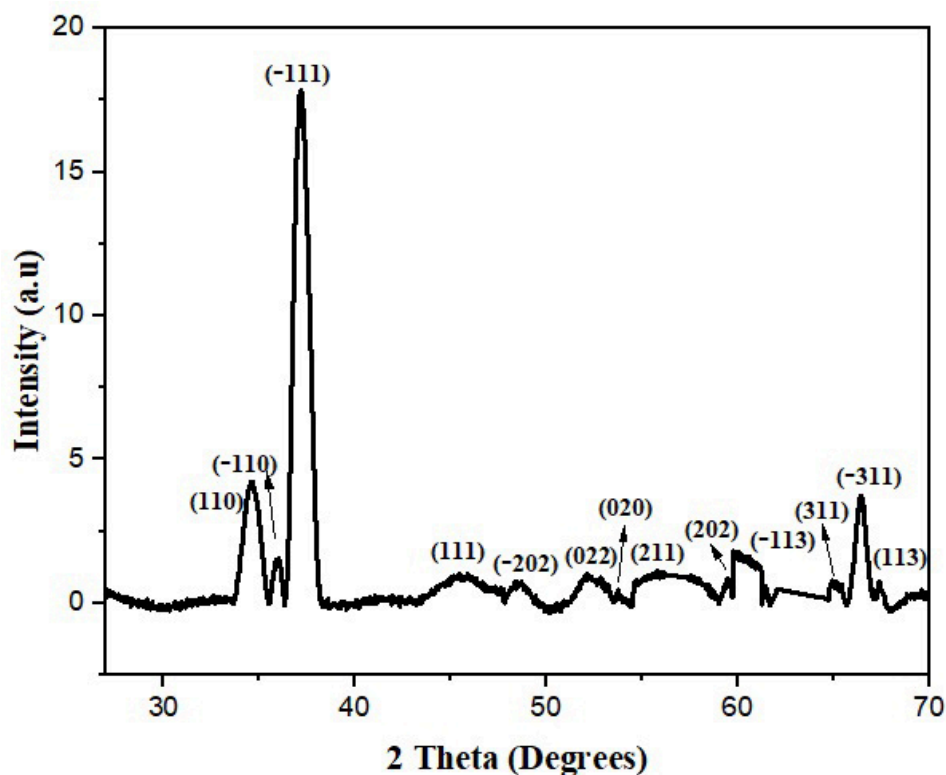


Figure 1. XRD diffractogram of biogenic CuO NPs (monoclinic CuO phase structure).

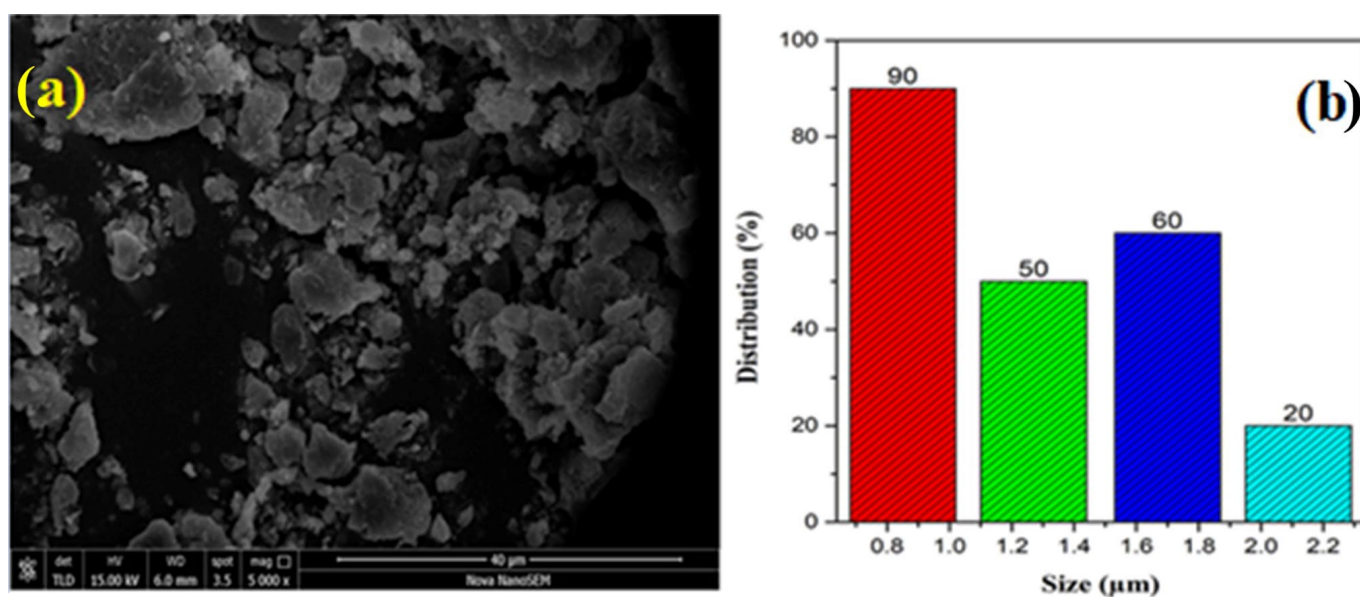


Figure 2. SEM image (a) and size distribution (b) of biogenic CuO NPs.

2.3. Fourier Transform Infrared (FTIR)

FTIR also allowed us to examine the composition and functional groups of bio-mechanochemically synthesized CuO NPs, from 400 to 4000 cm^{-1} . The strong vibrational bands found in the FTIR spectrum of CuO NPs (Figure 3) may be due to the biochemicals found in *Seriphidium oliverianum* extract (Figure S1), which capped the CuO NPs. Figure 3 shows a broad band at 3358 cm^{-1} , which matches the hydroxyl functional group of alcoholic or phenolic compounds found on the NPs surface. Another FTIR band at 1616 cm^{-1} corresponds to the aromatic bending vibrational frequency of the alkene group (C=C).

It may be due to the bio components of leaves, which play a role in the reduction and stabilization of NPs. The sharp band at 1352 cm^{-1} can be ascribed to frequencies of the C–H group of alkanes. The influential stretching band of C–O of the plant extract bio element alcoholic group is found at 1085 cm^{-1} . The bending vibration band of the aromatic group appears at 834 cm^{-1} . FTIR vibrational frequency ranges from 400 to 600 cm^{-1} , being attributed to Cu–O linkage, which confirms the formation of CuO NPs [72]. The functional groups associated with phytochemicals of *Seriphidium oliverianum* include glycoalkaloid, tropane alkaloid, and atropine, assigned to hydroxyl, aromatic, phenolic, and amino groups, which confirm the role of the plant extract as a reducing agent in the CuO NP synthesis.

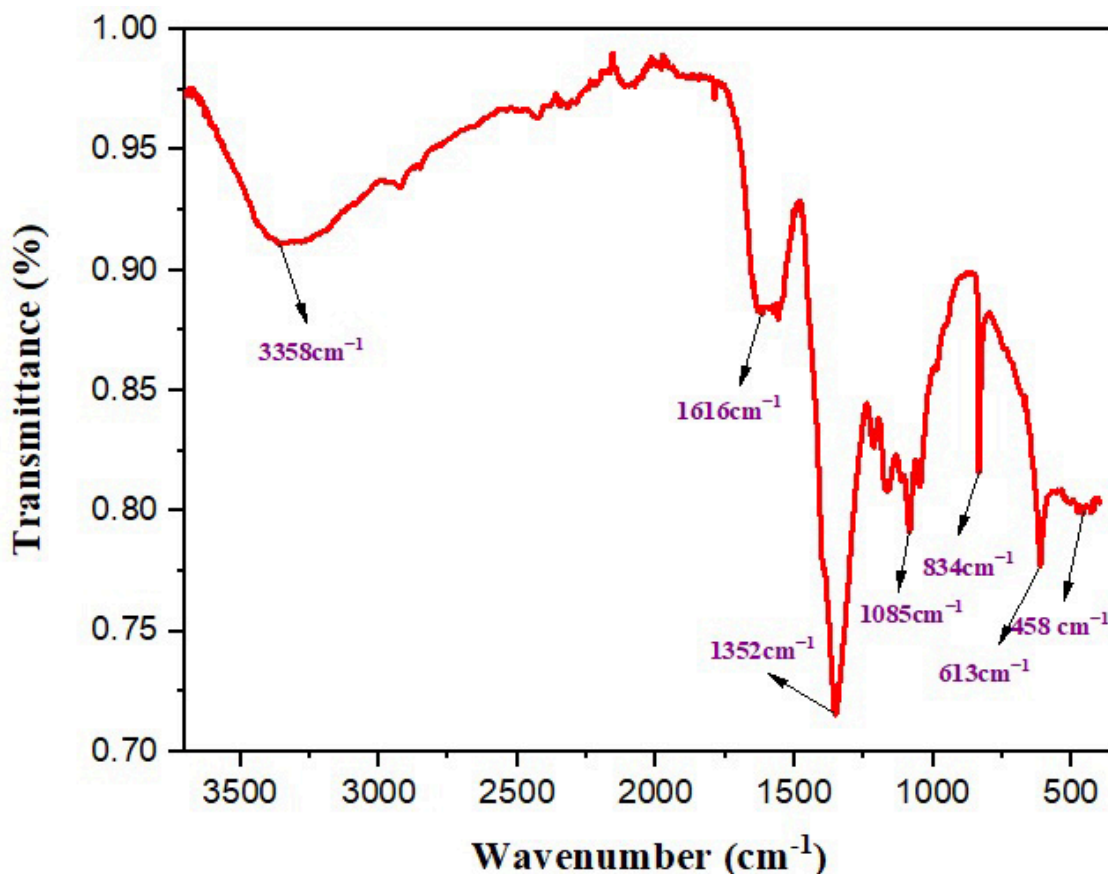


Figure 3. FTIR spectrum of biogenic CuO NPs.

2.4. UV-Visible Spectroscopy

Figure 4 shows the UV-Vis spectrum of CuO NPs, from 300 nm to 550 nm. It displays the expected absorption band at 324 nm for CuO NPs, and the band at 334 nm, due to the interband transition of Cu metal core electrons [73]. Bio components found in plant extracts play a role in the synthesis of stable CuO NPs [74]. Some aspects such as reaction time, temperature, concentration of precursor salt and aqueous leaf extract, and morphology of nanoparticles have an impact on the location of the absorption band in the UV-Vis spectrum. The sharp band also shows a high concentration of nanoparticles.

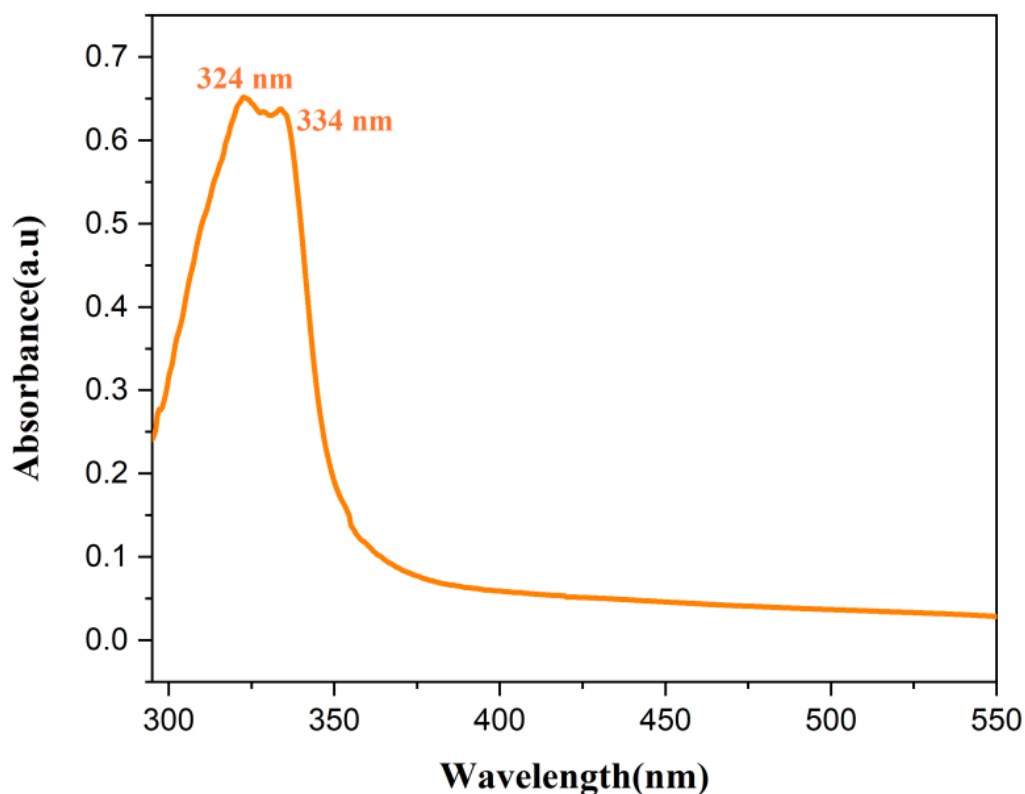


Figure 4. UV-vis spectrum of biogenic CuO NPs.

2.5. Photoluminescence Spectroscopy (PL)

PL allows us to reveal more details about exterior interstices, oxygen vacancies, surface flaws, optical emission facts, and photochemical characteristics of photocatalytic CuO NPs. The fluorescent process can also study the separation and transportation of electrons, the recombination process, and their effects on photocatalysis. The suggested mechanism of photoluminescence includes the movement of an electron from the valence to the conduction band after energy absorption via the generation of a hole. The recombination process occurs by shifting back the electron to the valence band with a simultaneous emission of energy. Furthermore, the small-sized particles are attributed to excellent facet fault and oxygen vacancies, resulting in a sharp luminescent peak [75].

The PL spectra of CuO NPs carried at 300 nm and 350 nm are shown in Figure 5. Two well-defined peaks are situated at 421 nm and 597 nm, for a wavelength of 300 nm (Figure 5a). The band at 421 nm is assigned to band edge-free excitons, and the band at 597 nm is attributed to bound excitons. The strong peak of PL spectra may be allocated to the small particle size and exterior defects. The intense band is also related to a high recombination rate. In Figure 5b, two distinct bands located at 450 nm and 699 nm are obtained by using a wavelength of 350 nm. These bands differ from those obtained at 300 nm (Figure 5a) because the excitation takes place at different wavelengths. Electron transformation occurs on different energy levels by absorbing different radiant energies and recombining them back to the valence band, with different conditions. So, the PL spectra covers different ranges. The intensity of band edge-free and bound excitons was found to be higher at a wavelength of 350 nm than at 300 nm. This confirms the existence of a UV adsorption band in the range of 324–334 nm, as previously mentioned in Section 3.4.

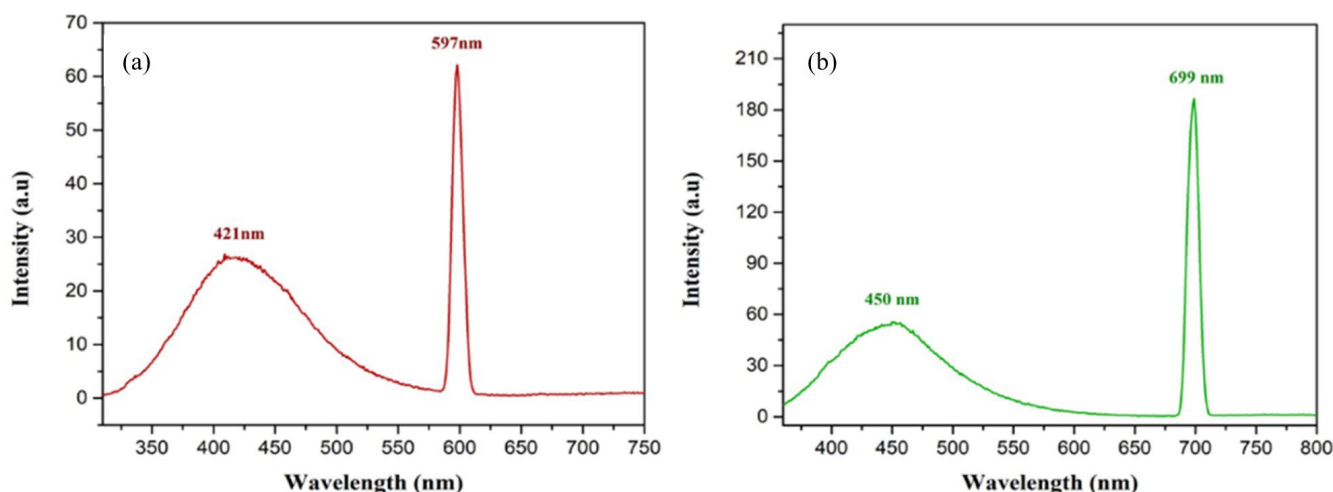


Figure 5. PL spectra of biogenic CuO NPs at: (a) 300 nm, (b) 350 nm.

2.6. A Plausible Mechanism for Biogenic CuO NPs

The bio reduction of the precursor salt starts instantly, and the formation of CuO NPs is demonstrated by the solution color changing from blue to dark brown. The biochemicals found in the plant extracts play a main role in the stabilization of CuO NPs [38].

It is expected that several functional groups, found in flavonoids, can be used as reductants and contribute to NP formation [76]. Moreover, the release of H atoms during the conversion of enol flavonoids into keto flavonoids reduces Cu ions into metal Cu NPs. Nevertheless, the precise mechanism for the synthesis of CuO NPs mediated by plant extracts is still unknown. It is believed that the depth of the nanoparticles' color, in an open environment, after one hour, can be attributed to oxidation, which is responsible for the formation of CuO NPs. Many factors might be involved, for e.g., it is possible that oxidation occurs due to environmental oxygen or biochemicals binding reduced metal ions before stabilization. Given electrostatic attraction, the ions of the metal oxide bind together forming NPs that are stabilized to prevent cluster formation. Despite the lack of a clear understanding of the mechanism, the use of plant extracts to synthesize nanoparticles is a promising approach due to its safe, environmentally friendly, and cost-effective nature. Figure 6 shows the proposed mechanism for CuO NP synthesis.

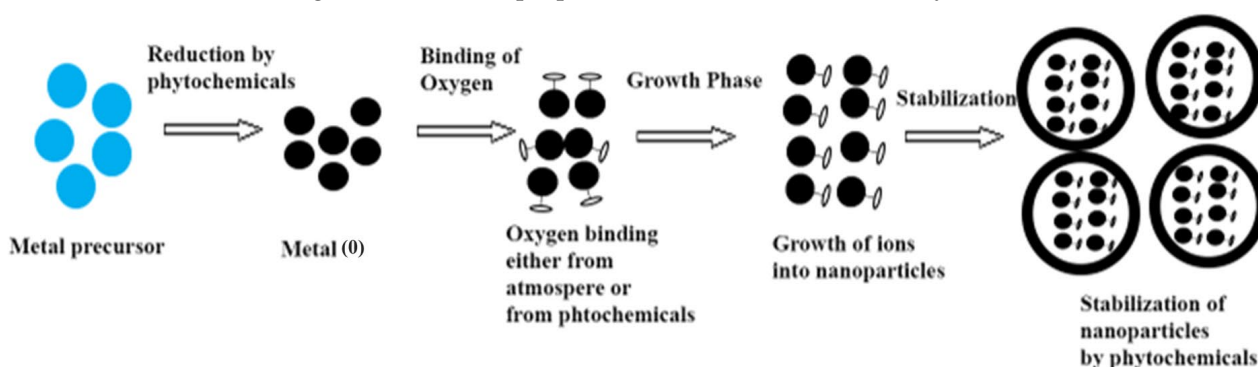


Figure 6. Mechanism of biogenic synthesis of CuO NPs.

2.7. Evaluation of Photocatalytic Activity

The photocatalytic degradation of MG and MO, in the presence of CuO NPs, is depicted in Figure 7. All parameters, namely irradiation time, light source, concentration of dyes, and catalyst were identical for all reactions. The degradation of dyes was evaluated using natural sunlight as the light source. The confined bandgap and high surface area significantly influenced the degradation activity. Absorption spectra were measured at regular

intervals using a UV-Vis spectrometer for all experiments. It was found that the intensity of the absorption band decreased as the illumination time under sunlight increased.

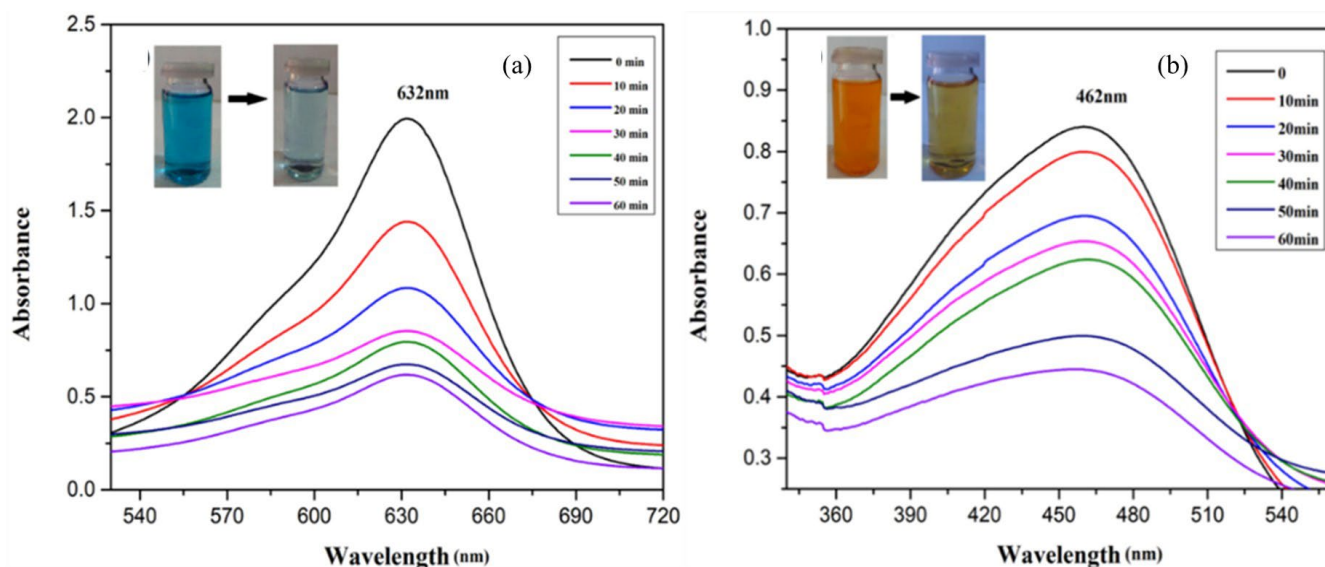


Figure 7. Absorption spectra of the dyes at different time intervals: (a) MG, (b) MO.

The main factors responsible for the decolorization of dyes were hydroxyl and oxy radicals, which degrade toxic contaminants formed when a hole–electron pair was created. Furthermore, the color of dyes simultaneously became lighter with time. Degradation efficiency for MG and MO was 65% and 65%, respectively, after 60 min of exposure to sunlight in the presence of a photocatalyst, as shown in Figure 8, Table 1. The rate constant is different for the two dyes, as they have different compositions and react differently. The higher the rate constant, the faster the reaction rate and vice versa.

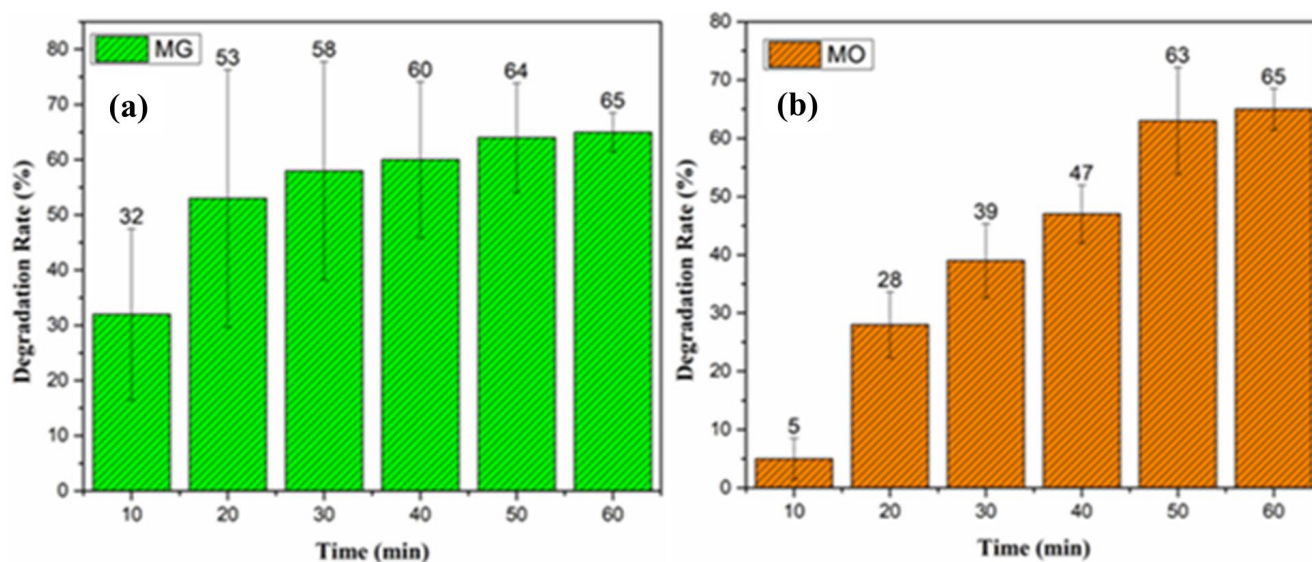


Figure 8. Degradation rate of (a) MG and (b) MO dyes.

Table 1. Degradation rates (%) and rate constants for photocatalytic degradation of dyes using biogenic CuO NPs.

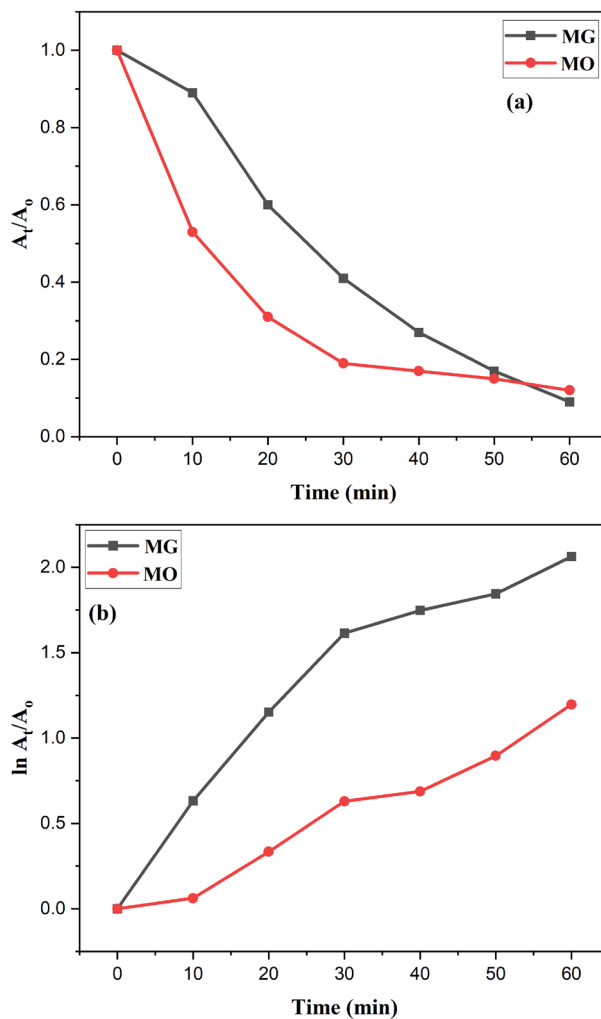
| Dyes | Degradation Rate% | Rate Constant (min^{-1}) |
|--------------------|-------------------|-------------------------------------|
| Methyl green (MG) | 65.231 | 0.0175285 |
| Methyl orange (MO) | 65.078 | 0.0175348 |

2.7.1. Kinetic Studies

In order to determine the degradation rate of organic compounds under optimal conditions, kinetic studies were conducted using the following relationship:

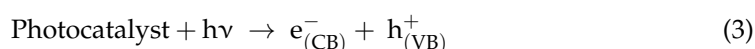
$$\ln A_0/A_t = kt \quad (2)$$

In the equation, “ A_0 ” is the absorbance of dyes at the time $t = 0$, “ A_t ” is the absorbance of dyes at time t , and “ k ” is the rate constant. Figure 9a shows the plot of A_0/A_t versus time, and Figure 9b shows $\ln A_0/A_t$ versus time. The slope of the graph represents the order of reaction (pseudo-first-order kinetics, which are attributable to the degradation of dyes) [77].

**Figure 9.** Kinetic results for dye degradation: (a) A_t/A_0 vs. time; (b) $\ln(A_t/A_0)$ vs. time.

2.7.2. Mechanism

The primary species involved in detoxifying dyes under sunlight irradiation were identified via an analysis of the process. Figure 10 depicts the proposed mechanism for the photocatalytic degradation of dyes. Nanomaterials with a small bandgap promote the creation of hole–electron pairs, as low absorption energy is necessary for electrons to move between the highest occupied molecular orbital (HOMO) to the lowest unoccupied molecular orbital (LUMO). When a catalyst absorbs, the absorption intensity is equal to the band gap energy. The electron movement occurs from the ground state to the excited state, creating a gap, valence band hole (h_{VB}^+), a free electron, and a conduction band electron (e_{CB}^-). The positive hole is a promising candidate to accept an electron from the pollutants in order to degrade them. Highly oxidizing species convert the water molecules into hydroxyl radicals (OH^\cdot), degrading the organic contaminants. Molecular oxygen combines with an electron and converts into a superoxide radical (O_2^\cdot) [78]. The process involved in the reduction of pollutants is given as follows:



It is believed that hollow spaces and hydroxyl radicals are the main reactive species during photocatalytic degradation of water-soluble dyes.

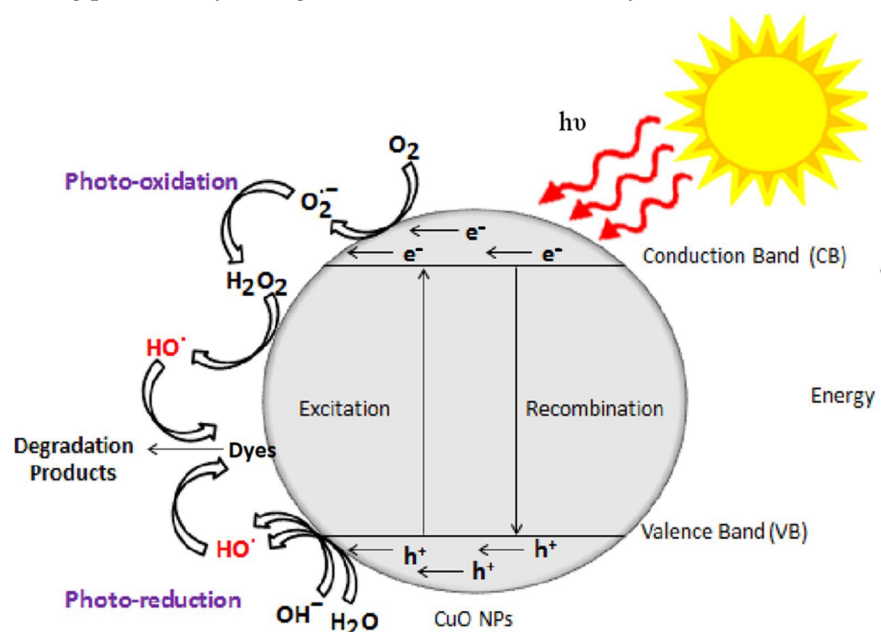


Figure 10. Schematic representation of photocatalytic degradation of dyes.

2.7.3. Parameters Affecting Photocatalytic Degradation

In order to achieve a remarkable photocatalytic activity, some features must be considered, such as the concentration of dyes and photocatalyst, the nature and structural morphology of the catalyst, irradiation time, and light source. The effect of the concentration of the dyes and catalyst loading on the degradation are given in Figures S2 and S3 of Supporting Information. The thermodynamic parameters such as ΔG° , ΔS° , and ΔH° are given in Figure S4 and Tables S1 and S2. The standard calculation deviation and R^2 value are also given in Tables S3 and S4.

An inhibited reaction is observed when the concentration of dyes is increased, as there is no interaction with the active sites of the catalyst. This is due to the lack of absorption of light intensity by the dyes and the difficulty of electrons being able to migrate to the photocatalyst, resulting in insufficient hydroxyl radicals for dye degradation, and thus poor results are obtained [79]. MG and MO dye solution (with a 10-ppm concentration) showed much better results, compared to solutions with 15 or 20 ppm.

Upon increasing the photocatalyst amount, more interaction sites become available, leading to an enhanced production of hole–electron couples and hydroxyl radicals for the efficient detoxification of organic pollutants. The design, morphology, and particle size of the catalyst are important aspects in photocatalytic degradation. Smaller-sized particles provide more active sites for the absorption of dyes, increasing the efficiency of the process [80]. In our case, a good result was obtained using 10 mg CuO NPs. The removal rate of 65% was achieved after 60 min of illumination. 100% efficiency could be obtained if the exposure time was increased.

Although there is no report in the literature on the degradation of mechanochemical synthesized CuO NPs (used for the first time in the present work), other processes were used by several authors. Table 2 provides a detailed comparison between our synthesized photocatalyst and other CuO-based materials reported in the literature.

Table 2. Comparative study of photocatalytic degradation of dyes using CuO based materials.

| Photocatalyst | Synthesis Method | Time (min) | Light Source | Dye | Degradation Rate | Ref. |
|---------------------|-------------------------------|------------|-----------------|--------|------------------|-----------|
| CuO NPs | Green Synthesis | 24 | UV light | MO | 96% | [81] |
| CuO NPs | Green Synthesis | 24 | UV light | MO | 96.4% | [82] |
| CuO NPs | Chemical Precipitation Method | 120 | UV light | MO | 90% | [83] |
| CuO Microspheres | Reflux Condensation Method | 93 | UV light | MO | 89.39% | [84] |
| | | 130 | UV light | MB | 92% | |
| CuO NPs | Green Synthesis | 60 | UV light | MO | 45.23% | [85] |
| | | 60 | Sunlight | MO | 31.95% | |
| CuO NPs | Green Synthesis | 60 | Sunlight | MO | 95% | [86] |
| CuO Nanorod | Hydrothermal Method | 90 | Sunlight | MO | 22% | [87] |
| CuO NPs | Co-precipitation Method | 120 | Xenon lamp | MO | 39% | [88] |
| | | 4 | | MO | 80% | |
| CuO NPs | Green Synthesis | 12 | Visible light | MB | 91% | [89] |
| | | 4 | | MR | 89% | |
| | | 4 | | EY | 97% | |
| CuO NPs | Green Synthesis | 120 | Solar light | NB | 93% | [90] |
| | | | | RY 160 | 81% | |
| CuO nano leaves | Hydrothermal Synthesis | 180 | UV light | MB | 89% | [91] |
| | | | | MV | 96% | |
| CuO NPs | Selective Method | 60 | UV light | MB | 81% | [92] |
| | | 120 | Sunlight | MB | 63% | |
| | | | | EY | 75.69% | |
| CuO NPs | Green Synthesis | 200 | Sunlight | Rh123 | 34.12% | [93] |
| | | | | MB | 71.06% | |
| CuO NPs | Precipitation Method | 15 | Visible source | MB | 74% | [94] |
| CuO Nanosheets | RT Synthesis | 6 | Sunlight | AR | 96.99% | [95] |
| CuO NPs | Green Synthesis | 90 | UV light source | RB | 98% | [96] |
| CuO NPs | Microwave-assisted method | 90 | Sunlight | MB | 99% | [97] |
| CuO NPs | Green Synthesis | 150 | Visible light | RB | 84% | [98] |
| | | | | MB | 93% | |
| CuO NPs | Electrochemical Method | 120 | Sunlight | MR | 90% | [99] |
| | | | | CR | 85% | |
| CuO NPs | Mechanochemical synthesis | 60 | Sunlight | MO | 65% | This work |
| CuO NPs | Mechanochemical synthesis | 60 | Sunlight | MG | 65% | This work |

Abbreviations: NB—Nile blue; RY160—Reactive yellow; CBB—Coomassie brilliant blue; EY—Eosin yellow; Rh123—rhodamine 123; MR—Methyl red; CR—Congo red; AR—Allura red; AB—Acid black 210; RT—room temperature.

Concerning MO, UV light is more effective, as degradation rates varying from 45.23% [85] up to 96.4% [82] are obtained, using CuO NPs prepared via green synthesis. Using sunlight, the efficiencies vary from 31.95% [85] to 95% [86] for CuO NPs prepared via green synthesis, but are much smaller for CuO nanorods prepared via a hydrothermal method (22%) [87]. Our materials were the first prepared through mechanochemical synthesis and achieved a 65% degradation of MO using sunlight. This value is within the values reported in the literature for other preparation methods, but our method is simpler.

Concerning MG, no studies were found in the literature using CuO materials. A comparison is given for CuO-based materials used for the degradation of other dyes, showing the potential of this metal oxide.

2.7.4. Recyclability of Photocatalyst

The reusability of CuO NPs for the degradation of dyes was also analyzed. After complete degradation, the photocatalyst was removed and washed with deionized water. Then the photocatalyst was sonicated for a half an hour in 50 mL of deionized water and dried in air for 24 h. The CuO photocatalyst was then used in several consecutive degradation reactions. Excellent results were obtained for up to five runs, revealing the stability of CuO NPs (Figure S5). After the fifth run, the photocatalytic activity of the material decreased, possibly due to the formation of intermediates during the degradation of dyes, as suggested by other authors [100]. Additionally, the particle surface might decay during the degradation process, leading to a reduction in the overall activity after repeated use. However, the reusability of photocatalysts is a crucial factor in practical applications, as it allows for the effective and sustainable removal of dyes from wastewater.

3. Material and Methods

All chemical and precursor materials were purchased from Sigma-Aldrich (99.99%) and handled as acquired without any further treatment. $\text{Cu}(\text{NO}_3)_2 \cdot 3\text{H}_2\text{O}$ was used as precursor material. All other chemicals were of analytical grade and used without any additional purification. Deionized water was utilized for the preparation of standard solutions.

3.1. Preparation of *Seriphidium Oliverianum* Leaf Extract

The leaves of *Seriphidium oliverianum* were washed with distilled water and dried in air for a few days. Dry leaves were mashed to form a powder, using a mortar and a pestle. 5 g of powder was dispersed in 50 mL of deionized water. After that, the dispersion was kept for 24 h and then heated at 70 °C for 30 min under continuous stirring, followed by filtration with filter paper (Whatman No. 1) twice to remove the suspended particles altogether. The obtained leaf extract was stored for further experiments. We used dry leaves because morphology, size, and shape may vary for fresh leaves [101]. Additionally, the amounts and types of flavonoid groups change, depending on thermal stability during leaf drying and extract preparation. Moreover, when fresh leaves are used, the UV spectra may not give a clear absorption band, compared to dry leaves.

3.2. Synthesis of CuO NPs

The required amount of copper nitrate was crushed into a fine powder, and 40 mL of plant extract was added ($[\text{Cu}] = 0.1 \text{ M}$), followed by continuous grinding for 3 h in an electric mortar grinder mill (Model 911MPEMG100) at 70 rpm speed. The formation of CuO NPs was noticed by a color change of the solution (from blue to dull, dark brown). After that, the solution was placed in an open-air atmosphere for one hour, intensifying the color from light to dark brown. The mixture was centrifuged at room temperature for 30 min at 4000 rpm and washed with deionized water to eliminate the excesses of leaf extract or precursor salt. The obtained CuO NPs were collected in a Petri dish and air-dried. The complete process is depicted in Figure 11.



Figure 11. Mechanochemical synthesis of biogenic CuO NPs.

3.3. Photocatalytic Experiments

The photocatalytic activity of photocatalytic CuO NPs was tested in the degradation of different dyes, namely, methyl green (MG) and methyl orange (MO), used as reference models (Table S5). The used sunlight came from a visible light source (average solar flux = $500 \text{ km h}^{-1} \text{ m}^{-2}$).

The reaction was initiated by adding 10 mg of CuO NPs to a 10-ppm solution (10 mgL^{-1}) of each dye. The mixture was stirred for 30 min in the dark in order to establish the adsorption–desorption equilibrium. A well-established spectrum of UV-vis absorption was seen in all experiments. Different bands were analyzed in the UV-Vis spectra for MG and MO, at 632 nm and 462 nm, respectively. The solution was stirred under sunlight irradiation, and 2 mL of suspension was withdrawn every 10 min, up to 60 min, to observe the absorption peak, which was considered the absorption of dyes at the time “t”, and analyzed with UV-Vis.

The following equation was used to measure the dye degradation [29].

$$\text{Degradation (\%)} = \left(\frac{A_0 - A_t}{A_0} \right) \times 100 \quad (4)$$

where A_0 is the absorbance at time = 0 and A_t is the absorbance at time = t.

3.4. Characterization

The optical characteristics of synthesized CuO NPs were analyzed via UV-vis spectroscopy (Cecil 7500 UV-Vis Spectrometer), from 295 to 550 nm. The structural and chemical composition of CuO NPs were characterized using a Fourier-transform infrared spectrophotometer (FTIR, Tensor 27) that had a vibrational frequency ranging from 400 to 4000 cm^{-1} . A powder X-ray Diffractometer (PXRD) (Bruker D8 Advance PXRD) with Cu-K α radiation source and wavelength λ equal to 1.540598 \AA was employed to determine the crystallite size, nature, and phase description of CuO NPs [27]. In addition, CuO NPs morphology was investigated with scanning electron microscopy (SEM) using a MIRA-III TESCON apparatus. Surface deformity, photochemical, optical, and structural analysis of the obtained products were characterized using a Photoluminescence (PL) spectrometer at wavelengths ranging from 300 nm to 350 nm (Cary Eclipse Agilent technology) [28].

4. Conclusions

This study successfully reported an unprecedented environment-friendly bio mechanochemical approach for the synthesis of CuO NPs, using an aqueous extract from the *Seriphidium oliverianum* leaves. The bio components present in leaves were used as stabilizing and reducing agents. PXRD analysis identified a monoclinic CuO phase with a crystallite size of 12.44 nm. PL spectra identified two separate bands at 421 nm and 597 nm, indicating the presence of oxygen vacancies within the CuO NPs, which improved the photocatalytic activity. The synthesized nanosized material effectively demonstrated catalytic activity

under sunlight illumination to degrade MG and MO dyes. The photocatalytic reduction followed a pseudo-first-order kinetics, with a removal rate of 65% for both MG and MO dyes. These promising results offered a new means for researchers to produce cost-effective and environmentally friendly photocatalysts to efficiently remove dyes from water.

Supplementary Materials: The following supporting information can be downloaded at: <https://www.mdpi.com/article/10.3390/catal13030502/s1>, Figure S1. FTIR spectrum of *Seriphidium oliverianum*; Figure S2: Effect of different concentrations of dyes on the degradation process; Figure S3. Effect of different concentrations of photocatalyst on the degradation process; Figure S4. Thermodynamic study of dyes degradation; Figure S5. Dyes degradation upon recycling of the photocatalyst; Table S1. Thermodynamic parameters for MG degradation on CuO NPs; Table S2. Thermodynamic parameters for MO degradation on CuO NPs; Table S3. RMSE calculations for degradation of MG; Table S4. RMSE calculations for degradation of MO. Table S5. Dyes used in this work. Refs. [102–105] are cited in supplementary materials.

Author Contributions: Conceptualization: M.B.T.; investigation: W.A., Mika Sillanpaa, S.A.C.C.; software: R.Y.; formal analysis: A.R. and T.J.; writing—original draft: S.A.; writing—review and editing: F.V., M.S., K.K., S.A.-F. and S.A.C.C., supervision: M.B.T., S.A.C.C. and I.B.; resources: I.B.; project administration: M.B.T. All authors have read and agreed to the published version of the manuscript.

Funding: This project was supported by Researchers Supporting Project Number (RSP-2023R7) King Saud University, Riyadh, Saudi Arabia. S.A.C.C. acknowledges support from FCT/MCTES (Fundação para a Ciência e Tecnologia and Ministério da Ciência, Tecnologia e Ensino Superior) through projects UIDB/50006/2020 and UIDP/50006/2020 and for the Scientific Employment Stimulus—Institutional Call (CEECINST/00102/2018). The authors thank The Islamia University of Bahawalpur for providing basic facilities.

Institutional Review Board Statement: Not applicable.

Informed Consent Statement: Not applicable.

Data Availability Statement: All data are present within the manuscript body.

Conflicts of Interest: There are no conflict of interest between the authors.

References

1. Zafar, A.; Ullah, S.; Majeed, M.T.; Yasmeen, R. Environmental pollution in Asian economies: Does the industrialisation matter? *OPEC Energy Rev.* **2020**, *44*, 227–248. [CrossRef]
2. Ukaogo, P.O.; Ewuzie, U.; Onwuka, C.V. Environmental pollution: Causes, effects, and the remedies. In *Microorganisms for Sustainable Environment and Health*; Elsevier: Amsterdam, The Netherlands, 2020; pp. 419–429.
3. Hasnat, G.T.; Kabir, M.A.; Hossain, M.A. Major environmental issues and problems of South Asia, particularly Bangladesh. *Handb. Environ. Mater. Manag.* **2018**, *2*, 1–40.
4. Reid, A.J.; Carlson, A.K.; Creed, I.F.; Eliason, E.J.; Gell, P.A.; Johnson, P.T.; Kidd, K.A.; MacCormack, T.J.; Olden, J.D.; Ormerod, S.J. Emerging threats and persistent conservation challenges for freshwater biodiversity. *Biol. Rev.* **2019**, *94*, 849–873. [CrossRef] [PubMed]
5. Hanafi, M.F.; Sapawe, N. A review on the water problem associate with organic pollutants derived from phenol, methyl orange, and remazol brilliant blue dyes. *Mater. Today Proc.* **2020**, *31*, A141–A150. [CrossRef]
6. Pavithra, K.G.; Jaikumar, V. Removal of colorants from wastewater: A review on sources and treatment strategies. *J. Ind. Eng. Chem.* **2019**, *75*, 1–19. [CrossRef]
7. Ismail, M.; Akhtar, K.; Khan, M.; Kamal, T.; Khan, M.A.; M Asiri, A.; Seo, J.; Khan, S.B. Pollution, toxicity and carcinogenicity of organic dyes and their catalytic bio-remediation. *Curr. Pharm. Des.* **2019**, *25*, 3645–3663. [CrossRef] [PubMed]
8. Choudhary, M.; Peter, C.; Shukla, S.K.; Govender, P.P.; Joshi, G.M.; Wang, R. Environmental issues: A challenge for wastewater treatment. In *Green Materials for Wastewater Treatment*; Springer: Berlin/Heidelberg, Germany, 2020; pp. 1–12.
9. Mehra, S.; Singh, M.; Chadha, P. Adverse impact of textile dyes on the aquatic environment as well as on human beings. *Toxicol. Int.* **2021**, *28*, 165–176.
10. Maheshwari, K.; Agrawal, M.; Gupta, A. Dye Pollution in Water and Wastewater. In *Novel Materials for Dye-Containing Wastewater Treatment*; Springer: Berlin/Heidelberg, Germany, 2021; pp. 1–25.
11. Nemiwal, M.; Zhang, T.C.; Kumar, D. Recent progress in g-C₃N₄, TiO₂ and ZnO based photocatalysts for dye degradation: Strategies to improve photocatalytic activity. *Sci. Total Environ.* **2021**, *767*, 144896. [CrossRef]

12. Reddy, C.V.; Reddy, K.R.; Harish, V.a.; Shim, J.; Shankar, M.; Shetti, N.P.; Aminabhavi, T.M. Metal-organic frameworks (MOFs)-based efficient heterogeneous photocatalysts: Synthesis, properties and its applications in photocatalytic hydrogen generation, CO₂ reduction and photodegradation of organic dyes. *Int. J. Hydrog. Energy* **2020**, *45*, 7656–7679. [[CrossRef](#)]
13. Ihsanullah, I.; Jamal, A.; Ilyas, M.; Zubair, M.; Khan, G.; Atieh, M.A. Bioremediation of dyes: Current status and prospects. *J. Water Process Eng.* **2020**, *38*, 101680. [[CrossRef](#)]
14. Rashid, R.; Shafiq, I.; Akhter, P.; Iqbal, M.J.; Hussain, M. A state-of-the-art review on wastewater treatment techniques: The effectiveness of adsorption method. *Environ. Sci. Pollut. Res.* **2021**, *28*, 9050–9066. [[CrossRef](#)] [[PubMed](#)]
15. Khan, S.; Bhardwaj, U.; Iqbal, H.M.; Joshi, N. Synergistic role of bacterial consortium to biodegrade toxic dyes containing wastewater and its simultaneous reuse as an added value. *Chemosphere* **2021**, *284*, 131273. [[CrossRef](#)] [[PubMed](#)]
16. Ahmad, A.; Mohd-Setapar, S.H.; Chuong, C.S.; Khatoun, A.; Wani, W.A.; Kumar, R.; Rafatullah, M. Recent advances in new generation dye removal technologies: Novel search for approaches to reprocess wastewater. *RSC Adv.* **2015**, *5*, 30801–30818. [[CrossRef](#)]
17. Piaskowski, K.; Świdarska-Dąbrowska, R.; Zarzycki, P.K. Dye removal from water and wastewater using various physical, chemical, and biological processes. *J. AOAC Int.* **2018**, *101*, 1371–1384. [[CrossRef](#)] [[PubMed](#)]
18. Kumar, P.S.; Joshiba, G.J.; Femina, C.C.; Varshini, P.; Priyadharshini, S.; Karthick, M.; Jothirani, R. A critical review on recent developments in the low-cost adsorption of dyes from wastewater. *Desalin. Water Treat* **2019**, *172*, 395–416. [[CrossRef](#)]
19. Adane, T.; Adugna, A.T.; Alemayehu, E. Textile industry effluent treatment techniques. *J. Chem.* **2021**, *2021*, 5314404. [[CrossRef](#)]
20. Ejraei, A.; Aroon, M.A.; Saravani, A.Z. Wastewater treatment using a hybrid system combining adsorption, photocatalytic degradation and membrane filtration processes. *J. Water Process Eng.* **2019**, *28*, 45–53. [[CrossRef](#)]
21. Rao, S.; AS, S.; Jayaprakash, G.K.; Swamy, M.M.; K, S.; Kumar, D. Plant seed extract assisted, eco-synthesized C-ZnO nanoparticles: Characterization, chromium(VI) ion adsorption and kinetic studies. *Luminescence*, 2022; *in press*. [[CrossRef](#)]
22. Carabineiro, S.A.C.; Thavorn-Amornsri, T.; Pereira, M.F.R.; Figueiredo, J.L. Adsorption of ciprofloxacin on surface-modified carbon materials. *Water Res.* **2011**, *45*, 4583–4591. [[CrossRef](#)]
23. Carabineiro, S.A.C.; Thavorn-amornsri, T.; Pereira, M.F.R.; Serp, P.; Figueiredo, J.L. Comparison between activated carbon, carbon xerogel and carbon nanotubes for the adsorption of the antibiotic ciprofloxacin. *Catal. Today* **2012**, *186*, 29–34. [[CrossRef](#)]
24. Silva, A.R.; Martins, P.M.; Teixeira, S.; Carabineiro, S.A.C.; Kuehn, K.; Cuniberti, G.; Alves, M.M.; Lanceros-Mendez, S.; Pereira, L. Ciprofloxacin wastewater treated by UVA photocatalysis: Contribution of irradiated TiO₂ and ZnO nanoparticles on the final toxicity as assessed by *Vibrio fischeri*. *Rsc Adv.* **2016**, *6*, 95494–95503. [[CrossRef](#)]
25. Chakraborty, R.; Asthana, A.; Singh, A.K.; Yadav, S.; Susan, M.A.; Carabineiro, S.A.C. Intensified elimination of aqueous heavy metal ions using chicken feathers chemically modified by a batch method. *J. Mol. Liq.* **2020**, *312*, 113475. [[CrossRef](#)]
26. Yadav, S.; Asthana, A.; Chakraborty, R.; Jain, B.; Singh, A.K.; Carabineiro, S.A.C.; Susan, M.A. Cationic Dye Removal Using Novel Magnetic/Activated Charcoal/beta-Cyclodextrin/Alginate Polymer Nanocomposite. *Nanomaterials* **2020**, *10*, 170. [[CrossRef](#)] [[PubMed](#)]
27. Yadav, S.; Asthana, A.; Singh, A.K.; Chakraborty, R.; Vidya, S.S.; Susan, M.A.; Carabineiro, S.A.C. Adsorption of cationic dyes, drugs and metal from aqueous solutions using a polymer composite of magnetic/beta-cyclodextrin/activated charcoal/Na alginate: Isotherm, kinetics and regeneration studies. *J. Hazard. Mater.* **2021**, *409*, 124840. [[CrossRef](#)] [[PubMed](#)]
28. Yadav, S.; Asthana, A.; Singh, A.K.; Chakraborty, R.; Vidya, S.S.; Singh, A.; Carabineiro, S.A.C. Methionine-Functionalized Graphene Oxide/Sodium Alginate Bio-Polymer Nanocomposite Hydrogel Beads: Synthesis, Isotherm and Kinetic Studies for an Adsorptive Removal of Fluoroquinolone Antibiotics. *Nanomaterials* **2021**, *11*, 568. [[CrossRef](#)] [[PubMed](#)]
29. Lilhare, S.; Mathew, S.B.; Singh, A.K.; Carabineiro, S.A.C. Calcium Alginate Beads with Entrapped Iron Oxide Magnetic Nanoparticles Functionalized with Methionine-A Versatile Adsorbent for Arsenic Removal. *Nanomaterials* **2021**, *11*, 1345. [[CrossRef](#)] [[PubMed](#)]
30. Martins, P.M.; Santos, B.; Salazar, H.; Carabineiro, S.A.C.; Botelho, G.; Tavares, C.J.; Lanceros-Mendez, S. Multifunctional hybrid membranes for photocatalytic and adsorptive removal of water contaminants of emerging concern. *Chemosphere* **2022**, *293*, 133548. [[CrossRef](#)]
31. Lilhare, S.; Mathew, S.B.; Singh, A.K.; Carabineiro, S.A.C. Aloe Vera Functionalized Magnetic Nanoparticles Entrapped Ca Alginate Beads as Novel Adsorbents for Cu(II) Removal from Aqueous Solutions. *Nanomaterials* **2022**, *12*, 2947. [[CrossRef](#)]
32. Chakraborty, R.; Asthana, A.; Singh, A.K.; Verma, R.; Sankarasubramanian, S.; Yadav, S.; Carabineiro, S.A.C.; Susan, M.A. Chicken feathers derived materials for the removal of chromium from aqueous solutions: Kinetics, isotherms, thermodynamics and regeneration studies. *J. Dispers. Sci. Technol.* **2022**, *43*, 446–460. [[CrossRef](#)]
33. Arif, M.; Shahid, M.; Irfan, A.; Nisar, J.; Wang, X.; Batool, N.; Ali, M.; Farooqi, Z.H.; Begum, R. Extraction of copper ions from aqueous medium by microgel particles for in-situ fabrication of copper nanoparticles to degrade toxic dyes. *Z. Für Phys. Chem.* **2022**, *236*, 1219–1241. [[CrossRef](#)]
34. Arif, M. Extraction of iron (III) ions by core-shell microgel for in situ formation of iron nanoparticles to reduce harmful pollutants from water. *J. Environ. Chem. Eng.* **2023**, *11*, 109270. [[CrossRef](#)]
35. Hajiani, M.; Sayadi, M.H.; Mozafarjalali, M.; Ahmadpour, N. Green Synthesis of Recyclable, Cost-Effective, Chemically Stable, and Environmentally Friendly CuS@ Fe₃O₄ Nanoparticles for the Photocatalytic Degradation of Dye. *J. Clust. Sci.* **2022**, *33*, 1–13. [[CrossRef](#)]

36. Ahmed, A.; Usman, M.; Yu, B.; Ding, X.; Peng, Q.; Shen, Y.; Cong, H. Efficient photocatalytic degradation of toxic Alizarin yellow R dye from industrial wastewater using biosynthesized Fe nanoparticle and study of factors affecting the degradation rate. *J. Photochem. Photobiol. B Biol.* **2020**, *202*, 111682. [[CrossRef](#)]
37. Safajou, H.; Ghanbari, M.; Amiri, O.; Khojasteh, H.; Namvar, F.; Zinatloo-Ajabshir, S.; Salavati-Niasari, M. Green synthesis and characterization of RGO/Cu nanocomposites as photocatalytic degradation of organic pollutants in waste-water. *Int. J. Hydrog. Energy* **2021**, *46*, 20534–20546. [[CrossRef](#)]
38. Aroob, S.; Taj, M.B.; Shabbir, S.; Imran, M.; Ahmad, R.H.; Habib, S.; Raheel, A.; Akhtar, M.N.; Ashfaq, M.; Sillanpää, M. In situ biogenic synthesis of CuO nanoparticles over graphene oxide: A potential nanohybrid for water treatment. *J. Environ. Chem. Eng.* **2021**, *9*, 105590. [[CrossRef](#)]
39. Muhammad, T.; Alkahtani, M.; Raheel, A.; Shabbir, S.; Fatima, R.; Aroob, S.; Noor, S.; Ahmad, R.; Alshater, H. Bioconjugate Synthesis of NiFe₂O₄ Using Juglans Regia Leaves Extract: Phytochemical Analysis, Optical Activity, Removal of Ciprofloxacin and Congo Red From Water. 2020; *Preprint from Research Square*. [[CrossRef](#)]
40. Mitra, M.; Ahamed, S.T.; Ghosh, A.; Mondal, A.; Kargupta, K.; Ganguly, S.; Banerjee, D. Polyaniline/reduced graphene oxide composite-enhanced visible-light-driven photocatalytic activity for the degradation of organic dyes. *ACS Omega* **2019**, *4*, 1623–1635. [[CrossRef](#)]
41. Feng, S.; Li, F. Photocatalytic dyes degradation on suspended and cement paste immobilized TiO₂/g-C₃N₄ under simulated solar light. *J. Environ. Chem. Eng.* **2021**, *9*, 105488. [[CrossRef](#)]
42. Karthikeyan, C.; Arunachalam, P.; Ramachandran, K.; Al-Mayouf, A.M.; Karuppuchamy, S. Recent advances in semiconductor metal oxides with enhanced methods for solar photocatalytic applications. *J. Alloy. Compd.* **2020**, *828*, 154281. [[CrossRef](#)]
43. Yadav, P.; Dwivedi, P.K.; Tonda, S.; Boukherroub, R.; Shelke, M.V. Metal and non-metal doped metal oxides and sulfides. In *Green Photocatalysts*; Springer: Berlin/Heidelberg, Germany, 2020; pp. 89–132.
44. TAŞDEMİRÇİ, T.Ç. Synthesis of copper-doped nickel oxide thin films: Structural and optical studies. *Chem. Phys. Lett.* **2020**, *738*, 136884. [[CrossRef](#)]
45. Naseem, T.; Durrani, T. The role of some important metal oxide nanoparticles for wastewater and antibacterial applications: A review. *Environ. Chem. Ecotoxicol.* **2021**, *3*, 59–75. [[CrossRef](#)]
46. Pourmoslemi, S.; Bayati, N.; Mahjub, R. Application of Box–Behnken design to optimize a sol-gel synthesis method for Ag and Zn doped CuO nanoparticles with antibacterial and photocatalytic activity. *J. Sol-Gel Sci. Technol.* **2022**, *104*, 319–329. [[CrossRef](#)]
47. Elysa, T.; Mulia, K.; Ibadurrohman, M.; Dewi, E.L. A comparative study of CuO deposition methods on titania nanotube arrays for photoelectrocatalytic ammonia degradation and hydrogen production. *Int. J. Hydrog. Energy* **2021**, *46*, 26873–26885. [[CrossRef](#)]
48. Forouzandeh, P.; Ganguly, P.; Dahiya, R.; Pillai, S.C. Supercapacitor electrode fabrication through chemical and physical routes. *J. Power Sources* **2022**, *519*, 230744. [[CrossRef](#)]
49. Khairy, M.; El-Shaarawy, M.; Mousa, M. Characterization and super-capacitive properties of nanocrystalline copper ferrite prepared via green and chemical methods. *Mater. Sci. Eng. B* **2021**, *263*, 114812. [[CrossRef](#)]
50. Gebremedhn, K.; Kahsay, M.H.; Aklilu, M. Green synthesis of CuO nanoparticles using leaf extract of catha edulis and its antibacterial activity. *J. Pharm. Pharmacol.* **2019**, *7*, 327–342. [[CrossRef](#)]
51. Galan, C.R.; Silva, M.F.; Mantovani, D.; Bergamasco, R.; Vieira, M.F. Green synthesis of copper oxide nanoparticles impregnated on activated carbon using Moringa oleifera leaves extract for the removal of nitrates from water. *Can. J. Chem. Eng.* **2018**, *96*, 2378–2386. [[CrossRef](#)]
52. El-Batal, A.I.; El-Sayyad, G.S.; Mosallam, F.M.; Fathy, R.M. Penicillium chrysogenum-mediated mycogenic synthesis of copper oxide nanoparticles using gamma rays for in vitro antimicrobial activity against some plant pathogens. *J. Clust. Sci.* **2020**, *31*, 79–90. [[CrossRef](#)]
53. Bukhari, S.I.; Hamed, M.M.; Al-Agamy, M.H.; Gazwi, H.S.; Radwan, H.H.; Youssif, A.M. Biosynthesis of copper oxide nanoparticles using Streptomyces MHM38 and its biological applications. *J. Nanomater.* **2021**, *2021*, 6693302. [[CrossRef](#)]
54. Kumar, J.A.; Krithiga, T.; Manigandan, S.; Sathish, S.; Renita, A.A.; Prakash, P.; Prasad, B.N.; Kumar, T.P.; Rajasimman, M.; Hosseini-Bandegharaei, A. A focus to green synthesis of metal/metal based oxide nanoparticles: Various mechanisms and applications towards ecological approach. *J. Clean. Prod.* **2021**, *324*, 129198. [[CrossRef](#)]
55. Mustapha, T.; Misni, N.; Ithnin, N.R.; Daskum, A.M.; Unyah, N.Z. A Review on Plants and Microorganisms Mediated Synthesis of Silver Nanoparticles, Role of Plants Metabolites and Applications. *Int. J. Environ. Res. Public Health* **2022**, *19*, 674. [[CrossRef](#)] [[PubMed](#)]
56. Waris, A.; Din, M.; Ali, A.; Ali, M.; Afridi, S.; Baset, A.; Khan, A.U. A comprehensive review of green synthesis of copper oxide nanoparticles and their diverse biomedical applications. *Inorg. Chem. Commun.* **2021**, *123*, 108369. [[CrossRef](#)]
57. El Shafey, A.M. Green synthesis of metal and metal oxide nanoparticles from plant leaf extracts and their applications: A review. *Green Process. Synth.* **2020**, *9*, 304–339. [[CrossRef](#)]
58. Siddiqi, K.S.; Husen, A. Current status of plant metabolite-based fabrication of copper/copper oxide nanoparticles and their applications: A review. *Biomater. Res.* **2020**, *24*, 11. [[CrossRef](#)] [[PubMed](#)]
59. Rehman, A.; Saeed, S.; Ahmed, A. Genetic diversity and population structure of Seriphidium Sub-genus of Artemisia from different terrains of Balochistan, Pakistan. *Biodiversitas J. Biol. Divers.* **2021**, *22*, 1826–1834. [[CrossRef](#)]

60. Shafiq, N.; Shafiq, S.; Rafiq, N.; Parveen, S.; Javed, I.; Majeed, H.N.; Mahmood, A.; Noor, N.; Anjum, A. Phytochemicals of the Seriphidium, economically and pharmaceutically important genus of Asteraceae family. *Mini-Rev. Org. Chem.* **2020**, *17*, 158–168. [[CrossRef](#)]
61. Abbas, A.; Naqvi, S.A.R.; Rasool, M.H.; Noureen, A.; Mubarik, M.S.; Tareen, R.B. Phytochemical analysis, antioxidant and antimicrobial screening of seriphidium oliverianum plant extracts. *Dose-Response* **2021**, *19*, 15593258211004739. [[CrossRef](#)]
62. Hano, C.; Abbasi, B.H. Plant-based green synthesis of nanoparticles: Production, characterization and applications. *Biomolecules* **2021**, *12*, 31. [[CrossRef](#)]
63. Fecheté, I.; Wang, Y.; Védrine, J.C. The past, present and future of heterogeneous catalysis. *Catal. Today* **2012**, *189*, 2–27. [[CrossRef](#)]
64. Munnik, P.; De Jongh, P.E.; De Jong, K.P. Recent developments in the synthesis of supported catalysts. *Chem. Rev.* **2015**, *115*, 6687–6718. [[CrossRef](#)]
65. Copéret, C.; Allouche, F.; Chan, K.W.; Conley, M.P.; Delley, M.F.; Fedorov, A.; Moroz, I.B.; Mougel, V.; Pucino, M.; Searles, K. Bridging the Gap between Industrial and Well-Defined Supported Catalysts. *Angew. Chem. Int. Ed.* **2018**, *57*, 6398–6440. [[CrossRef](#)]
66. Schüth, F. Control of solid catalysts down to the atomic scale: Where is the limit? *Angew. Chem. Int. Ed.* **2014**, *53*, 8599–8604. [[CrossRef](#)] [[PubMed](#)]
67. Schüth, F. Strukturierung fester Katalysatoren bis hinab zur atomaren Skala: Wo liegen die Grenzen? *Angew. Chem.* **2014**, *126*, 8741–8747. [[CrossRef](#)]
68. Gallei, M.; Schwab, E. Handbook of Heterogenous Catalysis. *Ertl. G* **2008**, *4*, 57–66.
69. Amrute, A.P.; De Bellis, J.; Felderhoff, M.; Schüth, F. Mechanochemical synthesis of catalytic materials. *Chem. A Eur. J.* **2021**, *27*, 6819–6847. [[CrossRef](#)]
70. Karge, H.G. *Handbook of Heterogeneous Catalysis*; Ertl, G., Knozinger, H., Schuth, F., Eds.; VCH: Weinheim, Germany, 2008.
71. Tsuzuki, T. Mechanochemical synthesis of metal oxide nanoparticles. *Commun. Chem.* **2021**, *4*, 143. [[CrossRef](#)]
72. Bonnia, N.N.; Fairuzi, A.A.; Akhir, R.M.; Yahya, S.M.; Rani, M.A.A.; Ratim, S.; Rahman, N.A.; Akil, H.M. Comparison study on biosynthesis of silver nanoparticles using fresh and hot air oven dried IMPERATA CYLINDRICA leaf. *IOP Conf. Ser. Mater. Sci. Eng.* **2017**, *290*, 012002. [[CrossRef](#)]
73. Usha, V.; Kalyanaraman, S.; Thangavel, R.; Vettumperumal, R. Effect of catalysts on the synthesis of CuO nanoparticles: Structural and optical properties by sol–gel method. *Superlattices Microstruct.* **2015**, *86*, 203–210. [[CrossRef](#)]
74. Sharma, J.K.; Akhtar, M.S.; Ameen, S.; Srivastava, P.; Singh, G. Green synthesis of CuO nanoparticles with leaf extract of Calotropis gigantea and its dye-sensitized solar cells applications. *J. Alloy. Compd.* **2015**, *632*, 321–325. [[CrossRef](#)]
75. Saif, S.; Tahir, A.; Asim, T.; Chen, Y. Plant mediated green synthesis of CuO nanoparticles: Comparison of toxicity of engineered and plant mediated CuO nanoparticles towards Daphnia magna. *Nanomaterials* **2016**, *6*, 205. [[CrossRef](#)]
76. Bhardwaj, R.; Bharti, A.; Singh, J.P.; Chae, K.H.; Goyal, N. Influence of Cu doping on the local electronic and magnetic properties of ZnO nanostructures. *Nanoscale Adv.* **2020**, *2*, 4450–4463. [[CrossRef](#)]
77. Shreyash, N.; Bajpai, S.; Khan, M.A.; Vijay, Y.; Tiwary, S.K.; Sonker, M. Green synthesis of nanoparticles and their biomedical applications: A review. *ACS Appl. Nano Mater.* **2021**, *4*, 11428–11457. [[CrossRef](#)]
78. Abebe, B.; Murthy, H.; Amare, E. Summary on Adsorption and Photocatalysis for Pollutant Remediation: Mini Review. *J. Encapsulation Adsorpt. Sci.* **2018**, *8*, 225–255. [[CrossRef](#)]
79. Zhao, J.; Chen, C.; Ma, W. Photocatalytic degradation of organic pollutants under visible light irradiation. *Top. Catal.* **2005**, *35*, 269–278. [[CrossRef](#)]
80. Kumar, A.P.; Bilehal, D.; Tadesse, A.; Kumar, D. Photocatalytic degradation of organic dyes: Pd- γ -Al₂O₃ and PdO- γ -Al₂O₃ as potential photocatalysts. *RSC Adv.* **2021**, *11*, 6396–6406. [[CrossRef](#)] [[PubMed](#)]
81. Sharma, S.; Kumar, K. Aloe-vera leaf extract as a green agent for the synthesis of CuO nanoparticles inactivating bacterial pathogens and dye. *J. Dispers. Sci. Technol.* **2021**, *42*, 1950–1962. [[CrossRef](#)]
82. Sharma, S.; Kumar, K.; Thakur, N.; Chauhan, S.; Chauhan, M.S. Eco-friendly Ocimum tenuiflorum green route synthesis of CuO nanoparticles: Characterizations on photocatalytic and antibacterial activities. *J. Environ. Chem. Eng.* **2021**, *9*, 105395. [[CrossRef](#)]
83. Pourmortazavi, S.M.; Rahimi-Nasrabadi, M.; Ahmadi, F.; Ganjali, M.R. CuCO₃ and CuO nanoparticles; facile preparation and evaluation as photocatalysts. *J. Mater. Sci. Mater. Electron.* **2018**, *29*, 9442–9451. [[CrossRef](#)]
84. Mageshwari, K.; Sathyamoorthy, R.; Park, J. Photocatalytic activity of hierarchical CuO microspheres synthesized by facile reflux condensation method. *Powder Technol.* **2015**, *278*, 150–156. [[CrossRef](#)]
85. Ikram, A.; Jamil, S.; Fasehullah, M. Green Synthesis of Copper Oxide Nanoparticles from Papaya/Lemon tea Extract and its Application in Degradation of Methyl Orange. *Mater. Innov.* **2022**, *2*, 115–122. [[CrossRef](#)]
86. Kayalvizhi, S.; Sengottaiyan, A.; Selvankumar, T.; Senthilkumar, B.; Sudhakar, C.; Selvam, K. Eco-friendly cost-effective approach for synthesis of copper oxide nanoparticles for enhanced photocatalytic performance. *Optik* **2020**, *202*, 163507. [[CrossRef](#)]
87. Sali, R.K.; Pujar, M.S.; Nadgir, A.; Sidarai, A.H. Photocatalytic activities of CuO nanorods over methyl orange: Hydrothermal method. In *AIP Conference Proceedings, Coimbatore, India, 17–18 July 2020*; AIP Publishing LLC: Baltimore, MD, USA, 2020.
88. Zeid, E.F.A.; Ibrahim, I.A.; Mohamed, W.A.A.; Ali, A.M. Study the influence of silver and cobalt on the photocatalytic activity of copper oxide nanoparticles for the degradation of methyl orange and real wastewater dyes. *Mater. Res. Express* **2020**, *7*, 026201. [[CrossRef](#)]

89. Sreeju, N.; Rufus, A.; Philip, D. Studies on catalytic degradation of organic pollutants and anti-bacterial property using biosynthesized CuO nanostructures. *J. Mol. Liq.* **2017**, *242*, 690–700. [[CrossRef](#)]
90. Singh, J.; Kumar, V.; Kim, K.-H.; Rawat, M. Biogenic synthesis of copper oxide nanoparticles using plant extract and its prodigious potential for photocatalytic degradation of dyes. *Environ. Res.* **2019**, *177*, 108569. [[CrossRef](#)]
91. Sonia, S.; Poongodi, S.; Kumar, P.S.; Mangalaraj, D.; Ponpandian, N.; Viswanathan, C. Hydrothermal synthesis of highly stable CuO nanostructures for efficient photocatalytic degradation of organic dyes. *Mater. Sci. Semicond. Process.* **2015**, *30*, 585–591. [[CrossRef](#)]
92. Akter, J.; Sapkota, K.P.; Hanif, M.A.; Islam, M.A.; Abbas, H.G.; Hahn, J.R. Kinetically controlled selective synthesis of Cu₂O and CuO nanoparticles toward enhanced degradation of methylene blue using ultraviolet and sun light. *Mater. Sci. Semicond. Process.* **2021**, *123*, 105570. [[CrossRef](#)]
93. Manikandan, D.B.; Arumugam, M.; Veeran, S.; Sridhar, A.; Krishnasamy Sekar, R.; Perumalsamy, B.; Ramasamy, T. Biofabrication of ecofriendly copper oxide nanoparticles using *Ocimum americanum* aqueous leaf extract: Analysis of in vitro antibacterial, anticancer, and photocatalytic activities. *Environ. Sci. Pollut. Res.* **2021**, *28*, 33927–33941. [[CrossRef](#)]
94. Benhadria, N.; Hachemaoui, M.; Zaoui, F.; Mokhtar, A.; Boukreris, S.; Attar, T.; Belarbi, L.; Boukoussa, B. Catalytic reduction of methylene blue dye by copper oxide nanoparticles. *J. Clust. Sci.* **2022**, *33*, 249–260. [[CrossRef](#)]
95. Nazim, M.; Khan, A.A.P.; Asiri, A.M.; Kim, J.H. Exploring rapid photocatalytic degradation of organic pollutants with porous CuO nanosheets: Synthesis, dye removal, and kinetic studies at room temperature. *ACS Omega* **2021**, *6*, 2601–2612. [[CrossRef](#)]
96. Rafique, M.; Shafiq, F.; Gillani, S.S.A.; Shakil, M.; Tahir, M.B.; Sadaf, I. Eco-friendly green and biosynthesis of copper oxide nanoparticles using *Citrofortunella microcarpa* leaves extract for efficient photocatalytic degradation of Rhodamin B dye from textile wastewater. *Optik* **2020**, *208*, 164053. [[CrossRef](#)]
97. Kannan, D.K.; Radhika, S.V.; Sadasivuni, K.K.; Ojiaku, A.A. Urvashi Verma, Facile fabrication of CuO nanoparticles via microwave-assisted method: Photocatalytic, antimicrobial and anticancer enhancing performance. *Int. J. Environ. Anal. Chem.* **2020**, *102*, 1095–1108. [[CrossRef](#)]
98. Shayegan Mehr, E.; Sorbiun, M.; Ramazani, A.; Taghavi Fardood, S. Plant-mediated synthesis of zinc oxide and copper oxide nanoparticles by using *ferulago angulata* (schlecht) boiss extract and comparison of their photocatalytic degradation of Rhodamine B (RhB) under visible light irradiation. *J. Mater. Sci. Mater. Electron.* **2018**, *29*, 1333–1340. [[CrossRef](#)]
99. Katwal, R.; Kaur, H.; Sharma, G.; Naushad, M.; Pathania, D. Electrochemical synthesized copper oxide nanoparticles for enhanced photocatalytic and antimicrobial activity. *J. Ind. Eng. Chem.* **2015**, *31*, 173–184. [[CrossRef](#)]
100. Pimol, P.; Khanidtha, M.; Prasert, P. Influence of particle size and salinity on adsorption of basic dyes by agricultural waste: Dried Seagrape (*Caulerpa lentillifera*). *J. Environ. Sci.* **2008**, *20*, 760–768. [[CrossRef](#)]
101. El-Berry, M.F.; Sadeek, S.A.; Abdalla, A.M.; Nassar, M.Y. Microwave-assisted fabrication of copper nanoparticles utilizing different counter ions: An efficient photocatalyst for photocatalytic degradation of safranin dye from aqueous media. *Mater. Res. Bull.* **2021**, *133*, 111048. [[CrossRef](#)]
102. Daneshvar, N.; Salari, D.; Khataee, A.R. Photocatalytic degradation of azo dye acid red 14 in water: Investigation of the effect of operational parameters. *J. Photochem. Photobiol. A Chem.* **2003**, *157*, 111–116.
103. Dhananasekaran, S.; Palanivel, R.; Pappu, S. Adsorption of methylene blue, bromophenol blue, and coomassie brilliant blue by α -chitin nanoparticles. *J. Adv. Res.* **2016**, *7*, 113–124. [[CrossRef](#)]
104. Kumar, A.; Pandey, G. A review on the factors affecting the photocatalytic degradation of hazardous materials. *Mater. Sci. Eng. Int. J* **2011**, *1*, 106. [[CrossRef](#)]
105. Moradi, S.E.; Haji Shabani, A.M.; Dadfarnia, S.; Emami, S. Effective removal of ciprofloxacin from aqueous solutions using magnetic metal–organic framework sorbents: Mechanisms, isotherms and kinetics. *Mater. Sci. Eng. Int. J* **2016**, *13*, 1617–1627. [[CrossRef](#)]

Disclaimer/Publisher’s Note: The statements, opinions and data contained in all publications are solely those of the individual author(s) and contributor(s) and not of MDPI and/or the editor(s). MDPI and/or the editor(s) disclaim responsibility for any injury to people or property resulting from any ideas, methods, instructions or products referred to in the content.